JOURNAL OF GUIDANCE, CONTROL, AND DYNAMICS
Vol. 28, No. 3, May–June 2005

Jet-Damping and Misalignment Effects During Solid-Rocket-Motor Burn

Jozef C. van der Ha* and Frank L. Janssens†
Spacecraft Design and Operations, Columbia, Maryland 21044

The present study provides an assessment of the dynamical processes that take place during the solid-rocket-motor (SRM) burn of a spin-stabilized spacecraft. We discuss the equations of motion for a system consisting of a rigid-body spacecraft and the gases in the SRM combustion chamber without specifying a model for the gas flow. In particular, we exploit the conservation of angular momentum flux from the solid propellant to the combustion gases leaving the system. We obtain a rotational equation that contains the jet-damping and misalignment effects in terms of the mass flow center and the mean exhaust velocity that summarize the action of the gases on the system for any flowfield. Compact analytical models are established that incorporate these effects. Piecewise linear approximations are adopted for the evolution of the system mass properties with respect to time during the SRM burn. We found that this technique is flexible and well suited for realistic time-varying system parameters. We illustrate the application of the model using the actual conditions of the CONTOUR spacecraft during its SRM burn on 15 August 2002.

I. Introduction

THE principal effects that influence the pointing stability of a spin-stabilized spacecraft during the burn of a solid rocket motor (SRM) are induced by misalignment and jet-damping torques. The former category is caused by errors in the SRM thrust vector direction and/or center-of-mass (c.m.) offsets induced by spacecraft balancing and alignment errors. The jet-damping torque originates from the resistance of the outflowing gases against a transverse rotation.

The earliest known reference to jet damping is by Rosser et al.[1] They derive an expression for the jet-damping moment of a non-spinning rocket and formulate this effect as restraining the yawing motion. They state correctly that this result remains valid for a spinning rocket where it restrains the conical yaw or the nutation in today's terminology. Of particular interest is their discussion of the lever arm appearing in the jet-damping moment. At first, they obtain a lever arm equal to the distance from the c.m. to the nozzle-exit plane. Subsequently, they make a case for a lever arm that equals the square root of the product of the distance from the c.m. to the nozzle-exit plane and the distance from the c.m. to the nozzle throat. This second model leads to a significantly smaller jet-damping effect for common motor configurations than other models. Their argument is that the transverse velocity of the gases can be equated to that of the solid parts only as long as their relative velocity is small. They propose that the argument should be settled by means of experiments, which however have never been carried out (as far as we know).

The next reference to jet damping is found in Davis et al. (Ref. 2, p. 33) "The existence of the jet-damping torque was first called to our attention by J. B. Rosser, who pointed out that if a rocket rotates about a transverse axis during burning, the gas must be accelerated laterally as it flows down the motor tube. The reaction on the motor tube tends to damp the rotation." This qualitative description of the jet-damping torque is unsurpassed in clarity. Their result for the jet-damping torque on p. 36 has the same structure as Rosser's but uses a different expression for the lever arm.

Received 14 July 2003; presented as Paper 2003-5328 at the AIAA Guidance, Navigation, and Control Conference, Austin, TX, 11–13 August 2003; revision received 25 September 2004; accepted for publication 28 October 2004.

*Consultant; jvdha@aol.com. Senior Member AIAA.
†Consultant; fjanssens@online.be.

More recently (for instance, Chobotov[3]), the meaning of jet damping has been extended to include also changes in spin rate caused by the dislocation of hydrazine fuel during thrusting. In the present paper, the term "jet damping" will be employed only in its original well-established meaning.

Thomson's classical book[4] provides models of the jet-damping torque for spinning and non-spinning rockets. He shows that the jet-damping effect is indeed stabilizing provided that the distance from the instantaneous spacecraft c.m. to the nozzle-exit plane exceeds the instantaneous transverse radius of gyration. It can readily be seen that a spacecraft with a normal geometrical shape satisfies this condition. Therefore, with the possible exception of a very compact spacecraft with a completely embedded solid-rocket-motor (SRM) nozzle, Thomson's criterion will be fulfilled in practice. He also shows that the jet-damping torque rotates at nutation frequency in the spacecraft frame. In his model, the complex three-dimensional gas flow is replaced by its contribution to the instantaneous rigid-body dynamics. The gases are assumed to flow through a nozzle having a number of orifices. This implies that the gases are in effect constrained to have the same spin rate as the solid spacecraft. Therefore, the jet-damping torque must necessarily possess a spin component (induced by the inertia-dot terms), and this would result in substantial changes in spin rate. However, these spin effects have not been observed in actual practice[5] and are thus not realistic. In his calculations Thomson[4] makes also the assumption that the radius of gyration remains constant.

Seames[6] treats Thomson's model with the transverse rotation as a vector rather than a complex number. Thomson and Reiter[5] reiterate the beneficial effect of jet damping on the nutation of a spinning rocket. Of most interest is their comparison of theoretical models with actual flight data of the Thor-Able third stage (during injection of Explorer VI). This showed an almost complete damping of the nutation and a negligible spin change at completion of the (37.7 s) burn. They conclude that a model containing the inertia-dot terms cannot possibly match the observed data. A model without these terms, on the other hand, gives a good correspondence for both the spin and transverse rate components. However, no physical explanations are offered.

Warner and Snyder[7] use Thomson's equations and calculate the spin evolution resulting from changes in the radius of gyration caused by propellant loss. This model finds of course considerable spin changes depending on the rate of change of the radius of gyration.

An interesting exchange ensued between Katz,[8] Papis,[9] and Warner and Snyder.[7] The first two authors call attention to the importance of the orifices in Thomson's model that force the gas to exit

with the same rotation rate as the solid part of the motor. The orifices are thus responsible for the change in angular momentum and for the spin effects. For an SRM with a single exit nozzle, this mechanism will be absent so[8] "there is no transfer of the spin component of the angular momentum between the gases and the rest of the system." Warner and Snyder[7] admit that their (i.e., Thomson's) model would indeed be more representative of liquid-propellant motors where the propellant is guided in pipes. All three papers stress the important role of viscosity in the dynamics of the gases. We do agree with this statement in as far as the full dynamics of the problem is concerned, but we recall that viscous effects cannot change the angular momentum as they are internal forces obeying the "action equals reaction" principle.

The summary by G. Tandon on jet damping[10] is consistent with the preceding remarks: in a solid motor with a single nozzle, "the exhaust gases carry away angular momentum equal to that of the fuel which was burned . . . since there is no time to exchange angular momentum." We will show in this paper that the argument is in fact independent of the fast transit time and of the type of flow. Tandon describes jet damping as "the phenomenon in which the rotation of the exhaust gases carries away a portion of the spacecraft angular momentum perpendicular to the nominal exhaust direction." The resulting jet-damping equation (from Keat and Shear[11]) leads to a full cancellation of the inertia-dot terms when the gases conserve their angular momentum and the jet-damping effect cannot lead to a change in spin rate. Wertz (see Ref. 10) also provides a useful overview of error sources that lead to disturbance torques during the SRM firing. A general numerical model is proposed for analyzing jet-damping effects. Furthermore, a number of actual in-flight observations of (nearly) constant spin rates during SRM burns are mentioned.

Cornelisse et al.[12] present the dynamical characteristics of an SRM burn from basic principles in a step-by-step approach. Newton's laws are adapted for application to variable-mass systems and for a spatial description of the gas flow (i.e., the Eulerian formulation as opposed to a particle or Lagrangian description). Standard tools from fluid dynamics[13–16] are injected into the dynamical equations, and all simplifying assumptions are clearly spelled out. When arriving at the scalar equations containing the jet-damping and misalignment terms (p. 79), they neglect the remaining integrals containing the gases using the argument that they are small. As a consequence, the inertia-dot terms do remain in their equations.

Flandro et al.[17] performed an impressive study of the gasdynamics during the SRM burn following the nutation growth observed in the STAR-48 motors. The general equations of motion are of a similar form as in Cornelisse et al.[12] but they are complemented by equations for the gas flow coupled to the motion of the solid part at the boundaries. They present an in-depth analysis of the gasdynamic effects produced by the Coriolis and relative moment integrals. They conclude that the interactions between the strong axial vortex and the solid part of the system can amplify the nutation for specific SRM configurations. This effect can lead to an unsteady (i.e., time-dependent) flow component. The mechanism they describe represents the reaction of the solid part of the SRM on the gas flow when the gases counteract the nutation. When this excitation occurs in a resonance condition (i.e., at the nutation frequency and in phase), the system can become unstable. The gasdynamic term containing this mechanism is part of the relative moment (volume integral). Needless to say that the ensuing calculations are very complex: indeed, they are at the limit of the capabilities of the computational-fluid-dynamics software codes.

Janssens[18] starts from the derivation of the equations of motion given by Cornelisse et al.[12] and identifies the terms that should cancel because of the conservation of angular momentum flux but exploits this property only for the spin component. His extended model contains two constants K_1 and K_2 representing the perturbing torques caused by the complex gasdynamics of the STAR-48 motor as described by Flandro et al.[17] He concludes that only K_1 plays a role in the nutation growth and that a better match with flight data might be achieved if K_1 were taken time dependent (for instance, proportional to the thrust acceleration).

Eke and Wang[19] establish the same general attitude equations [his Eq. (20)] as previous investigators. In Eq. (22) they transform the Coriolis moment similarly as done by Cornelisse et al.[12] and Janssens.[18] In their applications, they consider from the outset an axisymmetric steady flow for which the relative moment and part of the Coriolis moment vanish. As a consequence, the gas does not carry its angular momentum through the nozzle in the general equation (22) because the inertia-dot terms do not match up. In the idealized case of a burning rod, however, cancellation does occur. In a follow-on paper[20] axisymmetric flows without vortices in a cylinder (without nozzle) are studied. Under these assumptions, the radially outward burning case (progressive burning) becomes unstable when the radius of the cylinder exceeds its height by a factor of $\sqrt{\frac{8}{3}} \cong 1.63$. The continuation of this work in Wang and Eke[21] includes a steady vortex, which (in this type of model) affects only the spin rate. Recently, Mao and Eke[22] returned to the idealized case of a burning cylinder with uniformly varying mass.

Finally, Javorsek and Longuski[23] study the pointing error during the SRM burn and use a jet-damping model for comparison's sake. They employ Thomson's model but with a different lever arm for the jet damping.

The present paper builds on the insights offered by the preceding references. The model presented here exploits the fundamental conservation of the full angular momentum in all of its components. Instead of imposing simplifying assumptions on the flowfield characteristics within the SRM combustion chamber, we postulate that the angular momentum flux from the diminishing inertia of the solid part equals the angular momentum flux of the gases through the nozzle. The formal derivation makes use of the theory of a variable-mass system and leads naturally to expressions for the SRM thrust misalignment and the jet-damping torques. Furthermore, useful analytical solutions have been established in the special case of spacecraft with axisymmetric moments of inertia.

The model has been applied to the actual conditions of the CONTOUR spacecraft that was launched on 3 July 2002 and was lost during the firing of its SRM motor on 15 August 2002. It may be recalled that CONTOUR had a STAR-30 solid motor which does not have an embedded nozzle and has no history of nutation-growth problems caused by slag effects (as the STAR-48 motor had). CONTOUR's SRM extended far into the spacecraft, which produced a short lever arm for the jet damping torque. This coupled with the significant changes in the mass properties of the system lead to concerns about the spacecraft's stability during the SRM burn.

II. Jet-Damping Torque Model

The starting point for the derivation of our torque model is the well-established moment equation for a noninertial variable-mass system given, for instance, by Shames (Ref. 13, Sec. 5.10), Meirovitch (Ref. 24, Sec. 12.7), Cornelisse et al. (Ref. 12, Sec. 4.2), Flandro et al. (Ref. 17, Sec. 3.1), and Eke and Wang[19]:

$$\int_m \boldsymbol{r} \times \left\{ \ddot{\boldsymbol{R}} + 2\boldsymbol{\omega} \times \boldsymbol{V}_{xyz} + \dot{\boldsymbol{\omega}} \times \boldsymbol{r} + \boldsymbol{\omega} \times (\boldsymbol{\omega} \times \boldsymbol{r}) + \frac{\mathrm{D}(\boldsymbol{V}_{xyz})}{\mathrm{D}t} \right\} \mathrm{d}m = \boldsymbol{0} \tag{1}$$

Figure 1 shows the (x, y, z) frame, which is attached to the rigid part of the spacecraft and rotates with the instantaneous rate $\boldsymbol{\omega}$. The vector $\ddot{\boldsymbol{R}}$ in Eq. (1) denotes the acceleration of the origin of the (x, y, z) frame relative to the inertial reference. It is convenient to place the origin at the c.m. of the system under consideration, which consists of the rigid spacecraft plus the gases. The vector $\boldsymbol{r}$ denotes the instantaneous position of the particle dm with respect to the c.m. The first term in Eq. (1), that is,

$$\int_m (\boldsymbol{r} \times \ddot{\boldsymbol{R}})\, \mathrm{d}m$$

can now be evaluated as $m_{\text{system}}\,(\boldsymbol{r}_{\text{c.m.}} \times \ddot{\boldsymbol{R}}_{\text{c.m.}})$, which vanishes because of the definition of the c.m.:

$$\boldsymbol{r}_{\text{c.m.}} = \int_m \boldsymbol{r}\, \mathrm{d}m = \boldsymbol{0}$$

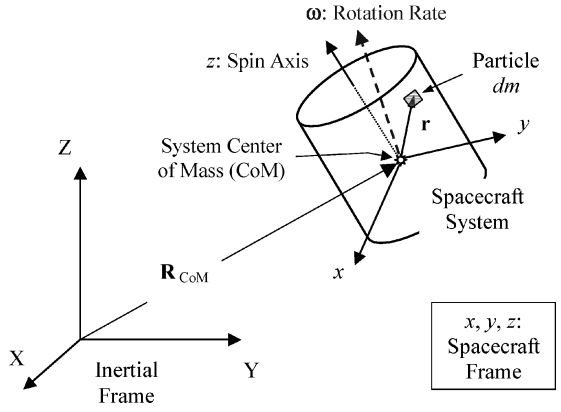

Fig. 1 Inertial and spacecraft reference frames; CoM, center of mass.

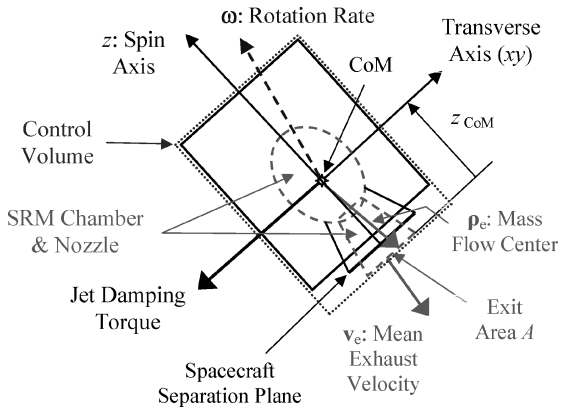

Fig. 2 Spacecraft configuration and dynamical properties; CoM, center of mass.

The relatively small velocity of the c.m. within the inertial frame during the SRM burn can be neglected in terms of its contribution to the equations of motion (Corneliss et al.,[12] p. 71). The velocity relative to the rotating (x, y, z) frame of a particle that happens to be at the position x, y, z within the spacecraft frame is $\boldsymbol{V}_{xyz}$. The derivative $\mathrm{D}(N)/\mathrm{D}t$ stands for the total or material rate of change of the arbitrary quantity N. The right-hand-side of Eq. (1) contains the torques caused by the external forces, which have been neglected here because of the dominance of the SRM thrust.

The integral

$$\int_m \{\ldots\}\,\mathrm{d}m$$

includes all particles that make up the variable-mass system at the time t. These particles are contained within the adopted control volume (Fig. 2), which is fixed to the rigid spacecraft (including the SRM casing and the remaining solid propellant) but contains also the gases within the SRM combustion chamber and nozzle at the time in question. Any potential additional effects induced by other nonrigid parts of the spacecraft such as hydrazine fuel will be ignored here.

Equation (1) expresses the conservation of angular momentum of the system because the interactions between the moving particles do not change the angular momentum due to Newton's action equals reaction law. We break up Eq. (1) in terms of the inertial moment $\boldsymbol{M}_{\mathrm{in}}$ and the apparent Coriolis and relative moments $\boldsymbol{M}_{\mathrm{Cor}}$ and $\boldsymbol{M}_{\mathrm{rel}}$:

$$\boldsymbol{M}_{\mathrm{in}} = \boldsymbol{M}_{\mathrm{Cor}} + \boldsymbol{M}_{\mathrm{rel}} \tag{2}$$

with

$$\boldsymbol{M}_{\mathrm{in}} = \int_m \boldsymbol{r} \times \{\dot{\boldsymbol{\omega}} \times \boldsymbol{r} + \boldsymbol{\omega} \times (\boldsymbol{\omega} \times \boldsymbol{r})\}\,\mathrm{d}m \tag{3a}$$

$$\boldsymbol{M}_{\mathrm{Cor}} = -2\int_m \boldsymbol{r} \times (\boldsymbol{\omega} \times \boldsymbol{V}_{xyz})\,\mathrm{d}m \tag{3b}$$

$$\boldsymbol{M}_{\mathrm{rel}} = -\int_m \boldsymbol{r} \times \frac{\mathrm{D}(\boldsymbol{V}_{xyz})}{\mathrm{D}t}\,\mathrm{d}m \tag{3c}$$

To deal with the variable-mass aspects during an SRM burn, we switch to a control volume approach. Each of the integrals in Eqs. (3) will now be analyzed separately.

A. Inertial Moment

The inertial moment $\boldsymbol{M}_{\mathrm{in}}$ in Eq. (3a) does not contain any terms that depend on the particles velocities $\boldsymbol{V}_{xyz}$ relative to the rigid-spacecraft frame. Therefore, the definition of the moment of inertia tensor $I(t)$ is directly applicable:

$$\boldsymbol{M}_{\mathrm{in}} = I(t)\dot{\boldsymbol{\omega}} + \boldsymbol{\omega} \times \{I(t)\boldsymbol{\omega}\} \tag{4}$$

The fact that the instantaneous control volume contains a different set of particles at different instants of time is irrelevant for the definition of the inertia tensor $I(t)$. We can now interpret Eq. (2) as follows: "The equations of rotational motion of a variable-mass system at time t can be written as those of a rigid body with mass m equal to the system mass at time t when, in addition to the true external forces and moments, two apparent (i.e., the Coriolis and relative) moments are applied." This interpretation is known as the solidification principle (Ref. 12, Sec. 3.4.4, and Ref. 24, Sec. 12.7).

The apparent moments in Eqs. (3b) and (3c) represent the actions of the gases on the rigid parts of the spacecraft during the SRM burn. The evaluation of these integrals is not straightforward as they require the solution of the Navier–Stokes equations, with boundary conditions given by the motion of the solid parts, for describing the motion of the gases inside the control volume. Hence, the complete equations of motion are given by Eq. (2) supplemented by the equations describing the motion of the gases (with their infinite number of degrees of freedom) coupled to the motion of the rigid spacecraft (see Flandro et al.[17] and Misterek et al.[25]). In practical applications, these integrals can often be evaluated by imposing reasonable simplifying assumptions about the flow characteristics.

B. Relative Moment

To evaluate the relative moment in Eq. (3c), we apply the Reynolds transport theorem (e.g., Shames[13] and Kuethe and Schetzer[15]) for expressing the total or material rate of change in terms of the rate of change of a flowfield within the selected control volume V with corresponding control surface A. We introduce the integral

$$\boldsymbol{h}_{\mathrm{rel}} = \int_m (\boldsymbol{r} \times \boldsymbol{V}_{xyz})\,\mathrm{d}m$$

which represents the relative angular momentum with respect to the spacecraft c.m. of the gas particles contained within the control volume. The Reynolds transport theorem is applicable to the relative moment in Eq. (3c) and produces the result

$$\boldsymbol{M}_{\mathrm{rel}} = -\int_m \frac{\mathrm{D}(\boldsymbol{r} \times \boldsymbol{V}_{xyz})}{\mathrm{D}t}\,\mathrm{d}m = -\frac{\mathrm{D}\boldsymbol{h}_{\mathrm{rel}}}{\mathrm{D}t}$$

$$= -\frac{\partial \boldsymbol{h}_{\mathrm{rel}}}{\partial t} - \int_A (\boldsymbol{r} \times \boldsymbol{V}_{xyz})(\boldsymbol{V}_{xyz} \cdot \boldsymbol{n})\mu\,\mathrm{d}A \tag{5}$$

Here, μ denotes the density of the gases within the infinitesimal volume $\mathrm{d}V$ and $\boldsymbol{n}$ represents the outward normal to the surface element $\mathrm{d}A$, which is an infinitesimal part of the nozzle exit area A (Fig. 2).

C. Coriolis Moment

The Coriolis moment in Eq. (3b) contains the relative velocity $\boldsymbol{V}_{xyz}$ of the particles so that it cannot be modeled as a rigidified system. Furthermore, the Reynolds transport theorem cannot be applied directly because $\boldsymbol{M}_{\mathrm{Cor}}$ is not a total derivative of some field quantity. Therefore, we will use $\mathrm{D}(I\boldsymbol{\omega})/\mathrm{D}t$ instead and transform it until $\boldsymbol{M}_{\mathrm{Cor}}$ shows up. This approach might look artificial but will turn out to be useful. We start from the product rule for derivatives

(valid for any type of derivative)

$$\frac{\partial}{\partial t}\{\boldsymbol{r}\times(\boldsymbol{\omega}\times\boldsymbol{r})\}=\boldsymbol{r}\times\left(\boldsymbol{\omega}\times\frac{\partial\boldsymbol{r}}{\partial t}\right)+\boldsymbol{r}\times\left(\frac{\partial\boldsymbol{\omega}}{\partial t}\times\boldsymbol{r}\right)+\frac{\partial\boldsymbol{r}}{\partial t}\times(\boldsymbol{\omega}\times\boldsymbol{r}) \tag{6}$$

After adding and subtracting the first term, we obtain

$$\frac{\partial}{\partial t}\{\boldsymbol{r}\times(\boldsymbol{\omega}\times\boldsymbol{r})\}=2\boldsymbol{r}\times\left(\boldsymbol{\omega}\times\frac{\partial\boldsymbol{r}}{\partial t}\right)+\boldsymbol{r}\times\left(\frac{\partial\boldsymbol{\omega}}{\partial t}\times\boldsymbol{r}\right)+\frac{\partial\boldsymbol{r}}{\partial t}\times(\boldsymbol{\omega}\times\boldsymbol{r})-\boldsymbol{r}\times\left(\boldsymbol{\omega}\times\frac{\partial\boldsymbol{r}}{\partial t}\right) \tag{7}$$

The last two terms of Eq. (7) can be combined by applying the vector identity $\boldsymbol{a}\times(\boldsymbol{b}\times\boldsymbol{c})+\boldsymbol{b}\times(\boldsymbol{c}\times\boldsymbol{a})+\boldsymbol{c}\times(\boldsymbol{a}\times\boldsymbol{b})=0$ with entries $\boldsymbol{a}=\boldsymbol{r}$, $\boldsymbol{b}=\boldsymbol{\omega}$, and $\boldsymbol{c}=\partial\boldsymbol{r}/\partial t$. We find after rearranging the terms

$$-2\boldsymbol{r}\times\left(\boldsymbol{\omega}\times\frac{\partial\boldsymbol{r}}{\partial t}\right)=-\frac{\partial}{\partial t}\{\boldsymbol{r}\times(\boldsymbol{\omega}\times\boldsymbol{r})\}+\boldsymbol{r}\times\left(\frac{\partial\boldsymbol{\omega}}{\partial t}\times\boldsymbol{r}\right)-\boldsymbol{\omega}\times\left(\boldsymbol{r}\times\frac{\partial\boldsymbol{r}}{\partial t}\right) \tag{8}$$

After integration over the system, the left-hand side will become identical to the moment $\boldsymbol{M}_{\mathrm{Cor}}$. The first term on the right-hand side is the rate of change $-\mathrm{D}(I\boldsymbol{\omega})/\mathrm{D}t$ to which the Reynolds transport theorem is applicable. For the middle term there is no distinction between integrating over the system and integrating over the control volume, and the result can readily be expressed in terms of the inertia tensor. The integral over the last term can still not be transformed to the control volume and remains an integral over the system. We finally obtain the following expression for $\boldsymbol{M}_{\mathrm{Cor}}$:

$$\begin{aligned}\boldsymbol{M}_{\mathrm{Cor}} &= -\frac{\mathrm{d}(I\boldsymbol{\omega})}{\mathrm{d}t}-\int_A\{\boldsymbol{r}\times(\boldsymbol{\omega}\times\boldsymbol{r})\}(\boldsymbol{V}_{xyz}\cdot\boldsymbol{n})\mu\,\mathrm{d}A\\ &\quad+I\frac{\mathrm{d}\boldsymbol{\omega}}{\mathrm{d}t}-\boldsymbol{\omega}\times\int_m(\boldsymbol{r}\times\boldsymbol{V}_{xyz}\,\mathrm{d}m\\ &= -\dot{I}\boldsymbol{\omega}-\int_A\{\boldsymbol{r}\times(\boldsymbol{\omega}\times\boldsymbol{r})\}(\boldsymbol{V}_{xyz}\cdot\boldsymbol{n})\mu\,\mathrm{d}A-\boldsymbol{\omega}\times\boldsymbol{h}_{\mathrm{rel}}\end{aligned} \tag{9}$$

Equation (9) has been derived without any specific assumptions on the characteristics of the flowfield within the control volume. Often (for instance, Shames[13]) the Coriolis moment is left as it stands in Eq. (3b) and later evaluated for a particular flowfield. The assumed flow characteristics must be relatively straightforward for the integration to be carried out in explicit terms (while ideally still including the relevant physics). For example, the most obvious type of flowfield is given by $\boldsymbol{V}_{xyz}=(0,0,\boldsymbol{V}_z)$ with a constant axial velocity V_z. Although the axial-flow model leads to an interesting result for the transverse dynamics,[25,26] the assumed flowfield suffers from the lack of angular momentum in the axial direction so the corresponding inertia-dot term produces an unrealistic spin-up.

D. Representative Flow Parameters

First, we introduce the mass flow parameter β (in units of kg/s), which is the rate of change of the system mass caused by the outflow of gases through the nozzle-exit plane A:

$$\beta=-\dot{m}=-\frac{\partial}{\partial t}\left\{\int_m\mathrm{d}m\right\}=\int_A(\boldsymbol{V}_{xyz}\cdot\boldsymbol{n})\,\mathrm{d}A \tag{10}$$

Next, we define two vector parameters that characterize the flowfield at the exit plane A, namely, the mass flow center $\boldsymbol{\rho}_e$ and the mean exhaust velocity $\boldsymbol{v}_e$ (Fig. 2) in units of m amd m/s, respectively:

$$\boldsymbol{\rho}_e=\left(\frac{1}{\beta}\right)\int_A\boldsymbol{r}(\boldsymbol{V}_{xyz}\cdot\boldsymbol{n})\mu\,\mathrm{d}A \tag{11a}$$

$$\boldsymbol{v}_e=\left(\frac{1}{\beta}\right)\int_A\boldsymbol{V}_{xyz}(\boldsymbol{V}_{xyz}\cdot\boldsymbol{n})\mu\,\mathrm{d}A \tag{11b}$$

The mass flow center $\boldsymbol{\rho}_e$ locates the effective exit point of the exhaust gases relative to the system c.m. The mean exhaust velocity $\boldsymbol{v}_e$ is responsible for the SRM thrust vector through $\boldsymbol{F}_{\mathrm{thrust}}=-\beta\boldsymbol{v}_e$. The thrust is known with good accuracy as demonstrated by the precision of a typical orbit injection. Under ideal conditions, that is, when there are no misalignments, when the flowfield is axisymmetric, and when there is no nutation, $\boldsymbol{\rho}_e$ and $\boldsymbol{v}_e$ will be pointing along the spacecraft centerline, which coincides with the nozzle axis.

We can split up the vector $\boldsymbol{r}$ appearing in the surface integrals as $\boldsymbol{r}=\boldsymbol{\rho}_e+\boldsymbol{\sigma}$ so that

$$\int_A\boldsymbol{\sigma}(\boldsymbol{V}_{xyz}\cdot\boldsymbol{n})\mu\,\mathrm{d}A$$

vanishes because of Eq. (11a). In general, $\boldsymbol{\rho}_e$ will not be pointing exactly along the nozzle axis and $\boldsymbol{\sigma}$ will not be perpendicular to $\boldsymbol{\rho}_e$ even though $\boldsymbol{\sigma}$ lies in the nozzle-exit plane.

E. Reduction of Moments

With the preceding definitions the relative moment in Eq. (5) and the Coriolis moment in Eq. (9) can be rewritten as

$$\boldsymbol{M}_{\mathrm{rel}}=-\beta(\boldsymbol{\rho}_e\times\boldsymbol{v}_e)-\int_A\{\boldsymbol{\sigma}\times\boldsymbol{V}_{xyz}\}(\boldsymbol{V}_{xyz}\cdot\boldsymbol{n})\mu\,\mathrm{d}A-\frac{\partial\boldsymbol{h}_{\mathrm{rel}}}{\partial t} \tag{12a}$$

$$\boldsymbol{M}_{\mathrm{Cor}}=-\dot{I}\boldsymbol{\omega}-\beta\{\boldsymbol{\rho}_e\times(\boldsymbol{\omega}\times\boldsymbol{\rho}_e)\}-\int_A\{\boldsymbol{\sigma}\times(\boldsymbol{\omega}\times\boldsymbol{\sigma})\}(\boldsymbol{V}_{xyz}\cdot\boldsymbol{n})\mu\,\mathrm{d}A-\boldsymbol{\omega}\times\boldsymbol{h}_{\mathrm{rel}} \tag{12b}$$

The torque component $-\beta\{\boldsymbol{\rho}_e\times\boldsymbol{v}_e\}$ originates from the thrust force $\boldsymbol{F}_{\mathrm{thrust}}=-\beta\boldsymbol{v}_e$ generated by the SRM. Under ideal circumstances, this torque component will vanish because ρ_e and $\boldsymbol{v}_e$ are pointing in the same direction. In the presence of misalignments, however, this torque can become significant because of the large magnitude of the SRM thrust and may affect the spacecraft stability.

The component $-\beta\{\boldsymbol{\rho}_e\times(\boldsymbol{\omega}\times\boldsymbol{\rho}_e)\}$ is usually called the jet-damping torque because it leads to a damping of the nutation. This term represents only a part of the Coriolis moment. In idealized flow models, it is usually the only term of the Coriolis moment remaining in the transverse dynamics. The lever arm of the jet-damping torque resulting from our model is ρ_e, which is the same as in Meyer.[26] Because the resulting lever arm depends on the assumed characteristics of the flowfield, many different expressions are in use. For instance, Misterek et al.[25] uses $\sqrt{(\rho_e^2-\rho_{\mathrm{bs}}^2)}$, where ρ_{bs} denotes the average axial coordinate of the burning surface. Javorsek and Longuski[23] use the distance from the c.m. to the throat of the nozzle. Flandro et al.[17] have an expression for the lever arm that contains also the diameter of the motor. We mentioned in the introduction the proposal by Rosser et al.[1] for yet another expression for the lever arm. The effects of the different lever arms on the resulting jet-damping magnitude depend on the specific system configuration.

We can recombine both remaining surface and volume integrals in Eqs. (12) by using the relations between the rate of change with respect to an inertial frame (denoted by $\mathrm{d}/\mathrm{d}t$) and the rate of change in the rotating spacecraft frame ($\partial/\partial t$):

$$\frac{\mathrm{d}\boldsymbol{\sigma}}{\mathrm{d}t}=\frac{\partial\boldsymbol{\sigma}}{\partial t}+\boldsymbol{\omega}\times\boldsymbol{\sigma} \tag{13}$$

$$\frac{\mathrm{d}\boldsymbol{h}_{\mathrm{rel}}}{\mathrm{d}t}=\frac{\partial\boldsymbol{h}_{\mathrm{rel}}}{\partial t}+\boldsymbol{\omega}\times\boldsymbol{h}_{\mathrm{rel}} \tag{14}$$

The resulting sum of the Coriolis and relative torques in Eqs. (12) can now be written in the final form:

$$\boldsymbol{M}_{\mathrm{cor}}+\boldsymbol{M}_{\mathrm{rel}}=-\dot{I}\boldsymbol{\omega}-\beta\{\boldsymbol{\rho}_e\times(\boldsymbol{\omega}\times\boldsymbol{\rho}_e)\}-\beta(\boldsymbol{\rho}_e\times\boldsymbol{v}_e)+-\int_A\left\{\boldsymbol{\sigma}\times\frac{\mathrm{d}\boldsymbol{\sigma}}{\mathrm{d}t}\right\}(\boldsymbol{V}_{xyz}\cdot\boldsymbol{n})\mu\,\mathrm{d}A-\frac{\mathrm{d}\boldsymbol{h}_{\mathrm{rel}}}{\mathrm{d}t} \tag{15}$$

The surface integral represents the angular momentum of the non-axial flow that is carried away through the nozzle exit. The $\mathrm{d}\boldsymbol{h}_{\mathrm{rel}}/\mathrm{d}t$ term describes the change in relative angular momentum of the gases

in the SRM chamber as seen in the inertial frame. Flandro et al.[17] observe that the gases spiral inward and form a vortex about the spin axis while still possessing the angular momentum that was originally contained in the solid propellant at the burning surface. Such behavior is fully consistent with a basic result from the dynamics of extended bodies, which states that angular momentum is conserved as long as the particles interact in a way that satisfies Newton's action equals reaction principle. Because changes in angular momentum may be produced only by discontinuities in the velocities in the burning surface, they should be very minor indeed.

The first term on the right-hand side of Eq. (15), that is, $-\dot{I}\boldsymbol{\omega}$, characterizes the flux of angular momentum that changes from the solid propellant to the gaseous flow at the burning surface within the SRM. This inertia-dot term by itself causes a decrease in the angular momentum of the spacecraft-SRM system as a result of the loss of propellant mass. However, we assume here that the angular momentum that is lost through the burning of the solid propellant will globally be transferred to the corresponding gases within the SRM combustion chamber. This observation can be formalized by postulating the fundamental assumption: "The angular momentum flux is fully conserved during the transformation from solid propellant to gases that takes place at the burning surface. This angular momentum is eventually carried out of the system by the gases through the exit nozzle." When also accounting for any momentum variations that may occur inside the combustion chamber, this statement can be expressed by the following identity:

$$-\dot{I}\boldsymbol{\omega} = \mathrm{d}\boldsymbol{h}_{\mathrm{rel}}/\mathrm{d}t + \int_A \{\boldsymbol{\sigma} \times \mathrm{d}\boldsymbol{\sigma}/\mathrm{d}t\}(\boldsymbol{V}_{xyz} \cdot \boldsymbol{n})\mu \, \mathrm{d}A \tag{16}$$

F. Resulting Moment Equation

We can simplify Eq. (15) with the help of the identity in Eq. (16) and find the final form of the Euler equations under the apparent Coriolis and relative torques:

$$I\dot{\boldsymbol{\omega}} + \boldsymbol{\omega} \times \boldsymbol{H} + \beta\{\boldsymbol{\rho}_e \times (\boldsymbol{\omega} \times \boldsymbol{\rho}_e)\} + \beta(\boldsymbol{\rho}_e \times \boldsymbol{v}_e) = 0 \tag{17}$$

This result describes the rotational motion of the spacecraft under the influence of the gases modeled by the vectors $\boldsymbol{\rho}_e$ and $\boldsymbol{v}_e$. In previous studies, equations like Eq. (17) have been obtained under much more restrictive assumptions (e.g., spin effects were assumed to be negligible or some of the integrals containing the gases were neglected under the argument that they are small), which prevented the precise cancellation of the terms shown in Eq. (16). If the complex gas flow problem (coupled to the motion of the rigid part) could be solved to deliver the detailed evolution of $\boldsymbol{\rho}_e$ and $\boldsymbol{v}_e$ throughout the burn, the solution of Eq. (17) would provide the exact evolution of the attitude motion. For simplicity, a steady flowfield may be assumed, which leads to constant vectors $\boldsymbol{\rho}_e$ and $\boldsymbol{v}_e$, and Eq. (17) would produce an approximate solution for the attitude motion.

The compact vector equation (17) can be expressed in components along the system's principal axes by expansion of the jet-damping torque $\{\boldsymbol{\rho}_e \times (\boldsymbol{\omega} \times \boldsymbol{\rho}_e)\}$ and the misalignment term $\boldsymbol{\rho}_e \times \beta\boldsymbol{v}_e \cong \boldsymbol{\rho}_e \times (-\boldsymbol{F}_{\mathrm{thrust}}) = -\boldsymbol{T}_{\mathrm{thrust}}$:

$$\begin{aligned} I_x\dot{\omega}_x + (I_z - I_y)\omega_z\omega_y + \beta\ell^2\omega_x &= T_{\mathrm{thrust,x}} \\ I_y\dot{\omega}_y - (I_z - I_x)\omega_z\omega_x + \beta\ell^2\omega_y &= T_{\mathrm{thrust,y}} \\ I_z\dot{\omega}_z + (I_y - I_x)\omega_x\omega_y &= T_{\mathrm{thrust,z}} \end{aligned} \tag{18}$$

Both the misalignment and jet-damping torque components can be considered constant (in any case, over an interval of one or a few seconds of time within the burn). The distance $\ell = |\boldsymbol{\rho}_e|$ represents the effective lever arm of the jet-damping torque.

III. Misalignment Torque Model

We refer here to the specific model used for the CONTOUR spacecraft, which was launched on 3 July 2002 and was equipped with a STAR-30BP SRM motor.

Equations (18) are referred to the spacecraft principal inertia axes. In reality, however, the thrust vector (which is aligned with $\boldsymbol{v}_e$) might not coincide with the principal z axis because of inertia imbalance effects (for instance, because of a difference in the remaining fuel between the tanks). There might also be errors in the thrust vector direction caused by imperfections within the SRM itself and due to mounting misalignments with respect to the spacecraft centerline. Furthermore, the lever arm might not be aligned in the nominal direction as a result of offsets in the effective thrust vector with respect to the system c.m. as illustrated in Wertz (Ref. 10, Fig. 17-6). Knauber[27] provides an extensive classification of the sources of misalignments. The errors considered here are the types E and F of his survey.

The pointing error of the SRM thrust vector $\boldsymbol{F}_{\mathrm{thrust}}$ in the system principal reference frame will be described by the half-cone angle δ and the constant but unknown phase angle β (Fig. 3). The components of the actual thrust vector within the principal frame are thus:

$$\boldsymbol{F}_{\mathrm{thrust}} = F_{\mathrm{thrust}}(\sin\delta\cos\beta, \sin\delta\sin\beta, \cos\delta)^T \tag{19}$$

The pointing error δ is made up of several independent error sources, including internal SRM-internal thrust direction error, SRM mechanical misalignments, as well as spacecraft imbalance effects. For CONTOUR the standard deviation of the angle δ is of the order of 0.1 deg, and its phase angle β is uniformly distributed over [0, 360] degs.

The magnitude of the SRM misalignment torque also depends on the position of the mass flow center $\boldsymbol{\rho}_e$, which is in the SRM nozzle-exit plane. Ideally, this vector would be pointing along the spacecraft principal z axis, but in practice the vector $\boldsymbol{\rho}_e$ can be misaligned in a direction normal to the z axis, that is, $\boldsymbol{\rho}_e = \ell\boldsymbol{u}_z + \boldsymbol{\sigma}_e$ (Fig. 3). The vector $\boldsymbol{\sigma}_e$ represents the small offset of the center of mass flow within the nozzle-exit plane. The standard deviation of the offset $\varepsilon = |\boldsymbol{\sigma}_e|$ is of the order of 1 mm (CONTOUR), and its phase angle α is uniformly distributed.

When expanding the force expression in Eq. (19) for small values of δ and the vector $\boldsymbol{\rho}_e$ for small ε we find the following result for the misalignment torque:

$$\boldsymbol{T}_{\mathrm{thrust}} = \boldsymbol{\rho}_e \times \boldsymbol{F}_{\mathrm{thrust}} = F_{\mathrm{thrust}}(\rho_x, \rho_y, \rho_z)^T$$

with

$$\rho_x \cong \varepsilon\sin\alpha - \delta\ell\sin\beta, \qquad \rho_y \cong \delta\ell\cos\beta - \varepsilon\cos\alpha$$

$$\rho_z \cong \varepsilon\delta\sin(\beta - \alpha) \tag{20}$$

The magnitude of the spin component induced by the misalignment torque is of second-order (with expected value 0 and standard deviation $\frac{1}{2}\sqrt{2\varepsilon\delta F_{\mathrm{thrust}}}$ Nm). Thus, the effect of the misalignment torque on the spin rate is negligible in practice, and for an axisymmetric spacecraft we have $\omega_z(t) = \Omega$. As an illustration, the relevant parameters of the CONTOUR spacecraft lead to an expected spin change of less than 0.1 rpm at the completion of the SRM burn. This result is consistent with actual observations quoted in Wertz (Ref. 10, p. 582).

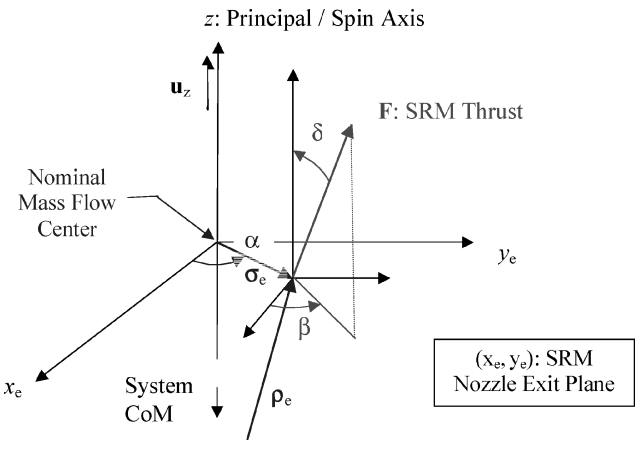

Fig. 3 SRM thrust vector in principal frame; CoM, center of mass.

IV. Motion Under Jet Damping Only

In this section, only the effect of the jet-damping torque will be presented. For simplicity, we assume here that the spacecraft has symmetric moments of inertia (i.e., $I = I_x = I_y$). It can be shown by means of a perturbation analysis that a small amount of asymmetry in the inertias will not affect the qualitative behavior of the analytical results.

After introducing the complex planar rotation rate $\boldsymbol{w} = \omega_x + j\omega_y$ (with j denoting the imaginary unit), the first two equations (18) can be combined:

$$\dot{\boldsymbol{w}} + \{\mathrm{d}(t) - j\Omega n(t)\}\boldsymbol{w} = 0 \tag{21}$$

with

$$d(t) = \beta\ell^2/I, \qquad n(t) = I_z/I - 1 \tag{22}$$

The jet-damping and nutation-frequency effects are characterized by the functions $d(t)$ and $n(t)$, respectively. Both functions take account of the time-varying nature of the mass properties and remain positive throughout the SRM burn for a spacecraft spinning about its maximum principal axis.

The general solution of Eq. (21) is

$$\boldsymbol{w}(t) = \boldsymbol{w}_0 \exp\{-D(t)\} \exp\{j\Omega N(t)\} \tag{23}$$

The (positive) functions $D(t)$ and $N(t)$ are defined by

$$D(t) = \int_0^t \mathrm{d}(s)\,\mathrm{d}s, \qquad N(t) = \int_0^t n(s)\,\mathrm{d}s \tag{24}$$

The result in Eq. (23) expresses two distinct effects: 1) the decrease in nutation angle caused by the jet-damping torque and modeled by $\exp\{-D(t)\}$ and 2) the variation in nutation frequency induced by the time-varying inertias and represented by $\exp\{j\Omega N(t)\}$.

A. Models for Mass Properties

The spacecraft mass properties during the SRM burn vary as complex and poorly known functions of time. There might be a discrepancy of a few percent between the predicted and the actual in-orbit inertias. Therefore, linear models for the system mass properties might be adequate in practice. In the case when accurate models for the mass properties are available that show a different behavior, the linear models presented here can readily be used successively with piecewise different values over each interval.

The instantaneous mass of the spacecraft-SRM system varies significantly during the SRM burn and will be modeled by the linear function

$$m(t) = m_0 - \beta t \tag{25}$$

Here, m_0 stands for the spacecraft-SRM mass at the start of the SRM burn and $\beta = -\dot{m}$. For simplicity the mass flow β will be taken constant during the SRM. For better precision the piecewise approach on the basis of a mass flow model should be employed.

The moments of inertia I and I_z decrease over the burn and are expressed by the following linear models:

$$I(t) = I_0(1 - \alpha t), \qquad I_z(t) = I_{z0}(1 - \gamma t) \tag{26}$$

The coefficients α and γ represent the rate of decrease of the moments of inertia and have units of sec^{-1}.

The jet-damping function $d(t)$ and the nutation-frequency function $n(t)$ can be expressed in the preceding functions:

$$d(t) = \beta\ell^2/I(t) = d_0/(1 - \alpha t) \tag{27}$$

$$n(t) = I_z/I - 1 = n_0\{1 + (\alpha - \gamma I_{z0}/I_0)t\}/(1 - \alpha t) \tag{28}$$

with n_0 the ratio of the nutation and spin frequency at the start of the SRM burn:

$$n_0 = I_{z0}/I_0 - 1 \tag{29}$$

After substituting the models for $d(t)$ and $n(t)$ into Eqs. (24) and integrating over time, we find

$$D(t) = -p\ell n[1 - \alpha t] \tag{30}$$

$$N(t) = n_0 t - E\{t + (1/\alpha)\ell n[1 - \alpha t]\} \tag{31}$$

The dimensionless parameters p and E stand for

$$p = d_0/\alpha = \beta\ell^2/(\alpha I_0); \qquad E = (I_{z0}/I_0)(1 - \gamma/\alpha) \tag{32}$$

The ratio of the instantaneous nutation frequency to the spin frequency for a variable-mass system should take account of the continuously varying mass properties and is defined as [Janssens,[18] Eq. (9)]

$$N(t)/t = (1/t)\int_0^t n(s)\,\mathrm{d}s = n_0 - E - E/(\alpha t)\,\ell n[1 - \alpha t] \tag{33}$$

The nutation/spin frequency ratio $N(t)/t$ depends on the full history of the mass properties from the start of the burn until time t. The frequency ratios before and after the burn should of course be modeled in accordance with the rigid-body results, $n_0 = I_{z0}/I_0 - 1$ and $n_f = I_{zf}/I_f - 1$.

B. Evolution of Nutation Angle

The nutation angle $\theta(t)$ during the SRM burn can be expressed (as long as the nutation remains relatively small) in terms of the absolute value of the complex rotation parameter $|\boldsymbol{w}(t)| = \{\omega_x^2 + \omega_y^2\}^{1/2}$ as follows:

$$\theta(t) = \arctan\{I(t)|\boldsymbol{w}(t)|/[I_z(t)\Omega]\}$$

$$\cong \theta_0\{I(t)/I_0\}\{I_{z0}/I_z(t)\}|\boldsymbol{w}(t)|/|\boldsymbol{w}_0| \tag{34}$$

The result $|\boldsymbol{w}(t)| = |\boldsymbol{w}_0|[1 - \alpha t]^p$ follows from Eqs. (23) and (30) so that the nutation damping ratio becomes

$$\theta(t)/\theta_0 = r_I(t)[I(t)/I_0]^p = r_I(t)|1 - \alpha t|^p \tag{35}$$

The constant exponent p is given in Eq. (32), and the inertia ratio r_I is

$$r_I(t) = \{I(t)/I_0\}/\{I_z(t)/I_{z0}\} = (1 - \alpha t)/(1 - \gamma t) \tag{36}$$

The result in Eq. (35) demonstrates the nutation damping property of the jet-damping torque. Because the ratio $I(t)/I_0 = 1 - \alpha t < 1$ and the exponent $p \gg 1$ (e.g., CONTOUR has $p \cong 16$), the nutation decreases exponentially. In case the inertia $I(t)$ decreases at a slower rate than $I_z(t)$, the ratio $r_I(t)$ in Eq. (36) would increase over time and might compensate for the decreasing effect of $[I(t)/I_0]^p$. In practice, however, the ratio $r_I(t)$ will be less than one [e.g., CONTOUR has $r_I(t) \cong 0.97$] or perhaps slightly larger than one. It is therefore improbable that the relatively small increase in $r_I(t)$ would be capable of canceling the strong exponential damping effect produced by the term $[I(t)/I_0]^p$.

In the case when a piecewise linear approach is adopted, the integration in Eqs. (23) and (24) should be performed with different parameters over each interval (t_{n-1}, t_n) (for $n = 1, \ldots, N$) with $t_0 = 0$ and $t_N = t_f$. It can be seen by iteration that the result in Eq. (35) becomes now

$$\theta_n/\theta_0 \cong r_n[I_n/I_{n-1}]^{p(n)}[I_{n-1}/I_{n-2}]^{p(n-1)}\ldots[I_1/I_0]^{p(1)} \tag{37}$$

The exponents $p(n)$ stand for $p(t_n)$, and the inertia ratio r_n is $r_I(t_n) = \{I_n/I_0\}/\{I_{zn}/I_{z0}\}$. The result of Eq. (37) collapses to the one in Eq. (35) for the case when $p(n) = p$ for all n.

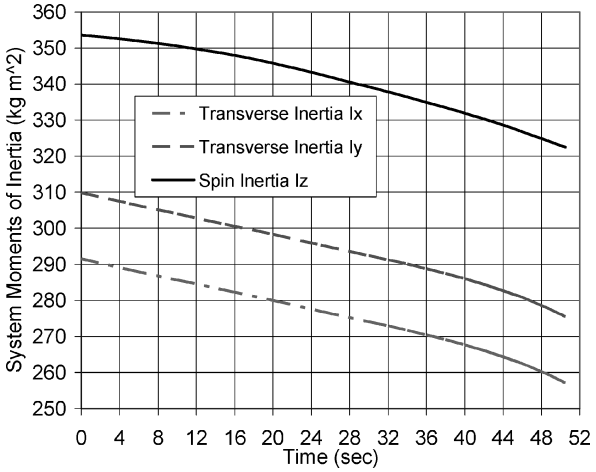

Fig. 4 System moments of inertia during burn.

V. Solution Including Misalignment

When including the (assumed constant) misalignment torque $\boldsymbol{T}_{\text{thrust}}$ of Eq. (20) in the differential Eq. (21) and introducing the complex torque parameter $\boldsymbol{T} = T_{\text{thrust,x}} + jT_{\text{thrust,y}}$, we find

$$\dot{\boldsymbol{w}} + \{\mathrm{d}(t) - j\Omega\, n(t)\}\boldsymbol{w} = \boldsymbol{T}/I(t) \tag{38}$$

Figure 4 indicates that the rates of change of the moments of inertia are fairly similar for the CONTOUR example. From now on we restrict ourselves to this special case, that is, $\dot{I}(t) \cong \dot{I}_z(t)$, which implies that $\alpha I_0 \cong \gamma I_{z0}$. This leads to $n(t) \cong n_0/(1-\alpha t)$ and $E \cong n_0$ in Eqs. (28) and (32). After also substituting $I(t)$ and $d(t)$ from Eqs. (26) and (27), we find for Eq. (38)

$$[1-\alpha t]\dot{\boldsymbol{w}} + (d_0 - j\Omega n_0)\boldsymbol{w} = \boldsymbol{T}/I_0 \tag{39}$$

The solution $\boldsymbol{w}(t)$ with initial condition $\boldsymbol{w}_0 = \boldsymbol{w}(t_0)$ can be expressed in the form

$$\boldsymbol{w}(t) = \boldsymbol{c} + (\boldsymbol{w}_0 - \boldsymbol{c})[1-\alpha t]^{p-jq} \tag{40}$$

with damping parameter $p = d_0/\alpha$ and frequency parameter $q = \Omega n_0/\alpha$. The imaginary constant $\boldsymbol{c}$ is defined by

$$\boldsymbol{c} = \boldsymbol{T}(d_0 + j\Omega n_0)\Big/\left\{I_0\left(d_0^2 + \Omega^2 n_0^2\right)\right\} \tag{41}$$

The result in Eq. (40) shows that $\boldsymbol{w}(t)$ describes a circular spiral in the complex plane. The spiral converges to its center at point $\boldsymbol{c}$ representing the "tip-off" angle induced by the misalignment torque. In practice, the magnitude of the imaginary part q of the exponent in Eq. (40) is much larger than that of the real part p (for CONTOUR we have a ratio of about 20) so that $\Omega n_0 \gg d_0$ and

$$\boldsymbol{c} \cong j\boldsymbol{T}/(I_0 \Omega n_0) \tag{42}$$

This confirms that the phase angle of the tip-off is roughly 90 deg ahead of that of the misalignment torque. For illustration, the CONTOUR parameters (at a 60 rpm spin rate) lead to a standard deviation of 1.6 deg for the magnitude of the tip-off angle.

In the absence of the misalignment torque $\boldsymbol{T}$, the center $\boldsymbol{c}$ in Eq. (40) vanishes, and the results of the preceding section are retrieved. The rotation axis converges (as a function of time) to the origin $\boldsymbol{c} = 0$ representing a pure spin without nutation. For a stable spinner (i.e., a spacecraft spinning about its maximum axis of inertia) the initial nutation will normally be negligible, and the jet damping will reduce this even further. Also for a spacecraft spinning about its minor axis, the jet-damping effect will in any case reduce the nutation.

In the absence of jet damping (consider, for instance, a thrust misalignment torque during a maneuver), the function $d(t)$ as well as the constant α will vanish so that p, q, and the result in Eq. (40) become ill-defined. It can readily be shown on the basis of Eq. (23) that in this case the solution corresponds to the well-known motion under a constant body-fixed torque:

$$\boldsymbol{w}(t) = \boldsymbol{c} + (\boldsymbol{w}_0 - c)\exp(j\Omega n_0 t) \tag{43}$$

The path of $\boldsymbol{w}(t)$ in the complex plane is now along a circle centered around the tip-off point $\boldsymbol{c}$. A visualization of the motion of the corresponding angular momentum and the resulting delta-velocity vectors for this case has been given in Fig. 2 of Oldenburg and Tragesser.[28]

VI. Results for CONTOUR

The models just established will now be illustrated in terms of the stability of the CONTOUR spacecraft during the SRM burn.

A. Mass Properties

The evolution of the system mass properties (i.e., mass, moments of inertias, and c.m. position) during the SRM burn are derived from a realistic model for the evolution of the SRM mass properties. The moments of inertia are calculated with respect to the instantaneous c.m. of the system (consisting of spacecraft, SRM casing, and remaining propellant). Figure 4 shows that the evolution of the inertias during the burn is close to linear at the start but becomes nonlinear near the end of the burn, in particular for the transverse inertias.

Figure 5 shows the evolution of the displacement of the c.m. (measured from the spacecraft separation plane; see Fig. 2) of the spacecraft-SRM system during the SRM burn. This result is obtained by considering the constant mass of the empty spacecraft in combination with the time-varying mass of the SRM motor (i.e., propellant plus casing). At the start of the burn, the SRM mass is close to that of the spacecraft itself (actually, about 10% larger), which makes the curve of the system c.m. roughly bisect the curves for the empty spacecraft and the SRM. It can readily be understood why the loss of the SRM propellant causes the system c.m. to first rise and then to fall again:

1) Because the propellant starts burning from the SRM bottom upward, both SRM and system c.m. rise at the start.

2) After the propellant has burned through the bulge of the SRM (Fig. 2), its c.m. drops, and the spacecraft mass dominates.

The movement of the spacecraft-SRM system c.m. during the burn leads to a time-dependent behavior of the jet-damping lever arm ℓ with a total variation of about 4.6 cm or close to 5% of its mean value $\langle \ell \rangle = 1.087$ m.

B. Effect of Jet Damping

First, we consider the simplest model, that is, the one based on representative mean values for the relevant parameters throughout the SRM burn:

$$\beta = 9.1857 \text{ kg/s}, \qquad \alpha = 2.261\,10^{-3}, \qquad \gamma = 1.721\,10^{-3}$$
$$n_0 = 0.1747, \qquad p = 15.939, \qquad q = 1.097 \tag{44}$$

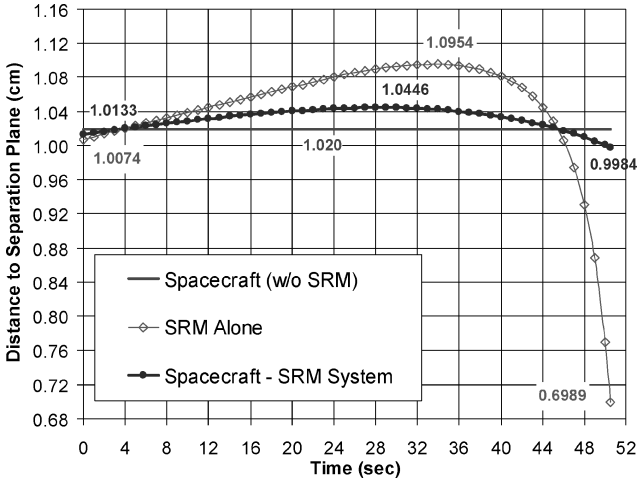

Fig. 5 Evolution of centers of mass during burn.

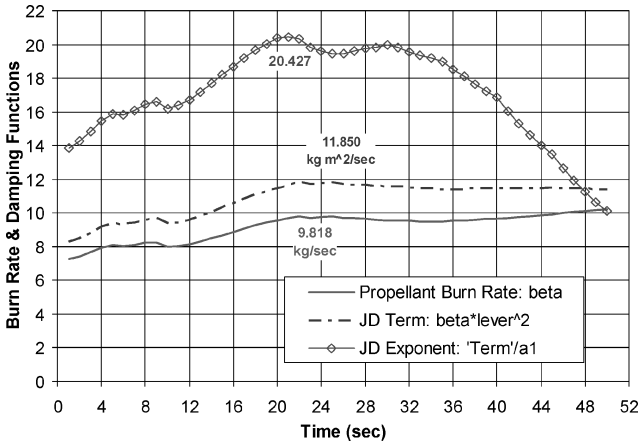

Fig. 6 Evolution of jet-damping parameters.

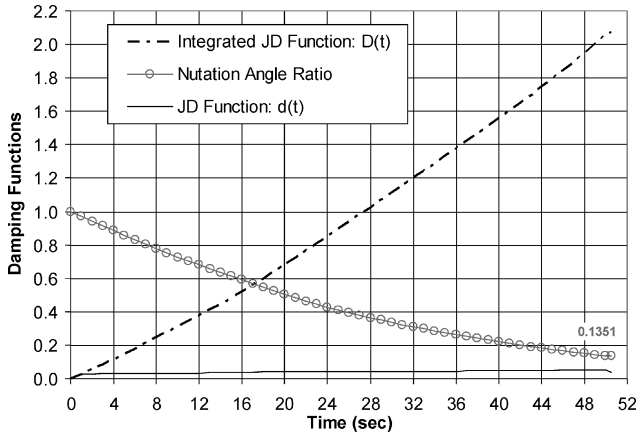

Fig. 7 Effect of jet damping on nutation angle.

The inertia ratio $r_I(t)$ varies between 1.0 at the beginning and $r_I(t_f) \cong 0.9701$ at the end of the burn at $t_f = 50.5$ s. The nutation damping at the end of the burn is predicted by Eq. (35) as follows:

$$\theta(t_f)/\theta_0 = r_I(t_f)[I(t_f)/I_0]^p = 0.9701(0.8858)^{15.939} = 0.1405 \tag{45}$$

Thus, the jet-damping torque reduces the initial nutation by as much as 85.95% at the end of the SRM burn.

Next, we employ the more accurate piecewise model in which all parameters are updated at the end of each interval. The 50.5 s of the SRM burn are divided into 50 intervals of 1 and 0.5 s for the last one. Figure 6 shows the evolution of the damping functions during the SRM burn. The exponent p shows a considerable variation over time. The main contributor to this is the unsteadiness in the rate of change of the transverse moment of inertia, that is, the parameter α [see Eq. (26) and Fig. 4] rather than variations in the mass flow or in the motion of the c.m.

Figure 7 shows the behavior of the time-varying jet-damping functions $d(t)$ and $D(t)$ during the SRM burn. Of most interest is the nutation angle, which will be reduced by as much as 86.49% at the end of the burn. The small difference of about 0.5% relative to the result of the simple model in Eq. (45) demonstrates (at least for the CONTOUR configuration) that the effectiveness of the nutation damping is not at all sensitive to the specific characteristics of the model used.

VII. Conclusions

The equations of motion for a spinning spacecraft during the solid-rocket-motor (SRM) burn have been formulated without making any assumptions about the nature of the gas flow. The jet-damping model is derived from a fundamental assumption about the dynamical interactions within the SRM, namely, that the angular momentum flux created by the burning propellant equals the flux carried by the combustion gases and the flux through the SRM nozzle. This approach leads naturally to explicit results for the jet-damping and misalignment torques expressed in terms of the mass flow center and the mean exhaust velocity.

The expressions for the torques are well suited for practical applications, in particular for investigating the stability of the spin axis pointing. The resulting differential equations have been solved analytically in the form of the product of a nutation-frequency function and a jet-damping function. Straightforward linear models for the system mass properties provide fairly accurate results for typical practical applications. These models are also suitable for piecewise use with different parameters in each interval in case a better accuracy is desired. The results indicate that the jet-damping torque has a stabilizing effect for any "normal" spacecraft configuration in terms of a significant nutation damping that will be effective throughout the SRM burn. The torque induced by thrust-vector misalignments produces a tip-off during the SRM burn that leads (after nutation damping) to a permanent change in spin axis pointing. Detailed simulations on the basis of actual values of the CONTOUR spacecraft demonstrate that about 86.5% of the nutation amplitude will be damped out at the end of its SRM burn. Furthermore, these results are not very sensitive to changes in the input parameters (at least for the CONTOUR example). The jet-damping model presented here (with a jet-damping lever arm to the exit plane) produces a more effective damping for the CONTOUR configuration than predicted by previous models.[1,2,4,5,17] Nevertheless, also the latter models lead to a significant reduction of the nutation and guarantee spacecraft stability during the SRM burn. Thus, we can conclude that jet-damping effects cannot possibly have caused the CONTOUR mishap.

References

[1]Rosser, J. B., Newton, R. R., and Gross, G. L., *Mathematical Theory of Rocket Flight*, McGraw–Hill, New York, 1947, pp. 19–23.

[2]Davis, L., Jr., Follin, J. W., and Blitzer, L., *Exterior Ballistics of Rockets*, van Nostrand, Princeton, NJ, 1958, pp. 33–36.

[3]Chobotov, V. A., *Spacecraft Attitude Dynamics and Control*, Krieger, Malabar, FL, 1991, Sec. 2.9.

[4]Thomson, W. T., *Introduction to Space Dynamics*, Wiley, New York, 1961; also Dover, New York, 1986, Sec.7.7–7.9.

[5]Thomson, W. T., and Reiter, G. S., "Jet Damping of a Solid Rocket: Theory and Flight Results," *AIAA Journal*, Vol. 3, No. 3, 1965, pp. 413–417.

[6]Seames, A. E., "Jet Damping of Symmetric Rockets," *AIAA Journal*, Vol. 3, No. 4, 1965, pp. 749, 750.

[7]Warner, G. G., and Snyder, V. W., "A Re-Evaluation of Jet Damping," *Journal of Spacecraft and Rockets*, Vol. 5, No. 3, 1968, pp. 364–366.

[8]Katz, P., "Comments on a Re-Evaluation of Jet Damping," *Journal of Spacecraft and Rockets*, Vol. 5, No. 3, 1968, p. 1246.

[9]Papis, T., "Comments on A Re-Evaluation of Jet Damping," *Journal of Spacecraft and Rockets*, Vol. 5, No. 3, 1968, pp. 1246, 1247.

[10]Tandon, G. K., "Modeling Torques Due to Orbit Maneuvers," *Spacecraft Attitude Determination and Control*, edited by J. R. Wertz, Reidel, Dordrecht, The Netherlands, 1978, Sec. 17.4, pp. 580–583.

[11]Keat, J., and Shear, M., "Apogee Motor Firing Dynamics Study for CTS," Computer Science Corp., 3000-05600-08TN, Silver Spring, MD, May 1974.

[12]Cornelisse, J. W., Schoeyer, H. F. T., and Wakker, K. F., *Rocket Propulsion and Spacecraft Dynamics*, Pitman, London, 1979, Chaps. 3–6.

[13]Shames, I. H., *Mechanics of Fluids*, 2nd ed., McGraw–Hill, New York, 1982, Sec. 5.10.

[14]Bird, R. B., Stewart, W. E., and Lightfoot, E. N., *Transport Phenomena*, Wiley, New York, 1960, Chap. 3.

[15]Kuethe, A. M., and Schetzer, J. D., *Foundations of Aerodynamics*, 2nd ed., Wiley, New York, 1964, Chap. 3.

[16]Sommerfeld, A., *Mechanics of Deformable Bodies, Lectures on Theoretical Physics*, Vol. 2, Academic Press, New York, 1964, Chap. 3.

[17]Flandro, G. A., Van Moorhem, W. K., Shorthill, R., Chen, K., Woolsey, M., Clayton, C. D., and Finlayson, P. A., "Fluid Mechanics of Spinning Rockets," Fluid Dynamics Lab., Air Force Rocket Propulsion Lab., AFRPL TR-86-072, Edwards AFB, CA, Jan. 1987.

[18]Janssens, F., "Jet Damping and Nutation Growth During the Burn of a Solid Rocket Motor Such as PAM-D," *ESA Journal*, Vol. 12, No. 3, 1988, pp. 273–288.

[19]Eke, F. O., and Wang, S., "Equations of Motion of Two-Phase Variable Mass Systems with Solid Base," *Journal of Applied Mechanics*, Vol. 61, No. 4, 1994, pp. 855–860.

[20]Eke, F. O., and Wang, S., "Attitude Behavior of a Variable Mass Cylinder," *Journal of Applied Mechanics*, Vol. 62, No. 4, 1995, pp. 935–940.

[21]Wang, S., and Eke, F. O., "Rotational Dynamics of Axisymmetric Variable Mass Systems," *Journal of Applied Mechanics*, Vol. 62, No. 4, 1995, pp. 970–974.

[22]Mao, T. C., and Eke, F. O., "Attitude Dynamics of a Torque-Free Variable Mass Cylindrical Body," *Journal of the Astronautical Sciences*, Vol. 48, No. 4, 2000, pp. 435–448.

[23]Javorsek, D., II, and Longuski, J. M., "Velocity Pointing Errors Associated with Spinning Thrusting Spacecraft," *Journal of Spacecraft and Rockets*, Vol. 37, No. 3, 2000, pp. 359–365.

[24]Meirovitch, L., *Methods of Analytical Dynamics*, McGraw–Hill, New York, 1970, Sec. 12.7.

[25]Misterek, D. L., Murdock, J. W., and Koshigoe, S., "Gas-Dynamic Flow in a Spinning, Coning Solid Rocket Motor," *Journal of Propulsion and Power*, Vol. 9, No. 1, 1993, pp. 35–42.

[26]Meyer, R. X., "Coning Instability of Spacecraft During Periods of Thrust," *Journal of Spacecraft and Rockets*, Vol. 33, No. 6, 1966, pp. 781–788.

[27]Knauber, R. N., "Thrust Misalignment of Fixed-Nozzle Solid Rocket Motors," *Journal of Spacecraft and Rockets*, Vol. 33, No. 6, 1966, pp. 794–799.

[28]Oldenburg, J. A., and Tragesser, S. G., "Minimizing the Effects of Transverse Torques During Thrusting for Spin-Stabilized Spacecraft," *Journal of Guidance, Control, and Dynamics*, Vol. 25, No. 3, 2002, pp. 591–595.